



## Optimization of ${}^6\text{LiF}:\text{ZnS}(\text{Ag})$ scintillator light yield using GEANT4

Y. Yehuda-Zada <sup>a,b</sup>, K. Pritchard <sup>c</sup>, J.B. Ziegler <sup>c</sup>, C. Cooksey <sup>c</sup>, K. Siebein <sup>c</sup>, M. Jackson <sup>d</sup>,  
C. Hurlbut <sup>d</sup>, Y. Kadmon <sup>b</sup>, Y. Cohen <sup>b</sup>, R.M. Ibberson <sup>c</sup>, C.F. Majkrzak <sup>c</sup>, N.C. Maliszewskij <sup>c,\*</sup>,  
I. Orion <sup>a</sup>, A. Osovizky <sup>c,e,f</sup>

<sup>a</sup> Department of Nuclear Engineering, Ben-Gurion University, Israel

<sup>b</sup> Nuclear Research Center Negev, Beer-Sheva, Israel

<sup>c</sup> National Institute of Standards and Technology (NIST), Gaithersburg, MD, United States

<sup>d</sup> Eljen Technology, Sweetwater, TX, United States

<sup>e</sup> Rotem Industries Ltd, Rotem Industrial Park, Israel

<sup>f</sup> University of Maryland, College Park, MD, United States

### ARTICLE INFO

#### Keywords:

GEANT4  
Neutron detector  
Simulation  
Scintillator  
WLS fibers

### ABSTRACT

A new cold neutron detector has been developed at the NIST Center for Neutron Research (NCNR) for the CANDoR (Chromatic Analysis Neutron Diffractometer or Reflectometer) project. Geometric and performance constraints dictate that this detector be exceptionally thin ( $\sim 2$  mm). For this reason, the design of the detector consists of a  ${}^6\text{LiF}:\text{ZnS}(\text{Ag})$  scintillator with embedded wavelength shifting (WLS) fibers. We used the GEANT4 package to simulate neutron capture and light transport in the detector to optimize the composition and arrangement of materials to satisfy the competing requirements of high neutron capture probability and light production and transport. In the process, we have developed a method for predicting light collection and total neutron detection efficiency for different detector configurations.

The simulation was performed by adjusting crucial parameters such as the scintillator stoichiometry, light yield, component grain size, WLS fiber geometry, and reflectors at the outside edges of the scintillator volume. Three different detector configurations were fabricated and their test results were correlated with the simulations. Through this correlation we have managed to find a common photon threshold for the different detector configurations which was then used to simulate and predict the efficiencies for many other detector configurations. New detectors that have been fabricated based on simulation results yielding the desired sensitivity of 90% for 3.27 meV ( $5 \text{ \AA}$ ) cold neutrons.

The simulation has proven to be a useful tool by dramatically reducing the development period and the required number of detector prototypes. It can be used to test new designs with different thicknesses and different target neutron energies.

### 1. Introduction

Neutron diffraction is used to determine the atomic and/or magnetic structure of a material. It can be applied to study crystalline solids, gasses, liquids or amorphous materials. CANDoR is an instrument which will use a collimated polychromatic neutron beam incident on the sample and a bank of energy-analyzing channels to collect the scattered radiation [1]. Each of the energy analyzing channels consists of a sequential array of 54 highly oriented pyrolytic graphite (HOPG) crystals arranged at different takeoff angles with respect to the incoming scattered neutrons. Neutrons with energies matched to the Bragg angle of each crystal are diffracted into an associated neutron detector. If

that neutron detector used is exceedingly thin ( $<2$  mm), more such energy analyzing channels can be placed adjacent to one another in the instrument detector package.

Both the thinness of the detector and the worldwide shortage of  ${}^3\text{He}$  gas rule out the use of gas filled proportional counters. A viable alternative is to use slabs of  ${}^6\text{LiF}:\text{ZnS}(\text{Ag})$  in which wavelength shifting fibers are embedded to produce the scintillation light and transport it to a photodetector [2–5]. Our design is described in detail in a separate article [6] (Fig. 1).

${}^6\text{LiF}:\text{ZnS}(\text{Ag})$  based scintillators contain two principal ingredients.  ${}^6\text{LiF}$  serves as the neutron converter with a high cross section (940

\* Corresponding author.

E-mail address: [Nicholas.Maliszewskij@nist.gov](mailto:Nicholas.Maliszewskij@nist.gov) (N.C. Maliszewskij).

Barns) for the neutron capture process  ${}^6\text{Li}(n,\alpha){}^3\text{H}$ . When a neutron is captured in the  ${}^6\text{Li}$ , a 2.06 MeV alpha particle and a 2.74 MeV triton are ejected in opposite directions (with a total kinetic energy of 4.78 MeV) [3,7–9].

The ZnS(Ag) serves as the scintillating material, with a theoretical light yield of  $\sim 100,000$  Photons/MeV [10]. However, ZnS(Ag) manufacturers typically report a lower light yield of about 50,000 Photons/MeV. When the alpha and triton particles excite the ZnS(Ag), photons at a peak wavelength of 450 nm are emitted. Wavelength shifting fibers embedded in the scintillator conduct the scintillation light to the light sensor.

The net neutron detection sensitivity (the fraction of neutrons passing through the detector which are successfully discriminated) is governed by the neutron capture probability and by the measurability of the scintillation light signature. For a finite scintillator volume such as that needed for this application, selecting the appropriate ratio of the active components is a matter of optimizing these two properties.

The scintillator volume should have enough  ${}^6\text{LiF}$  to give the scintillator high neutron capture efficiency, and there also should be an appropriate amount of ZnS(Ag) to generate enough photons capable of reaching the photosensor [11–13]. The alpha and triton particles travel only a few microns in the scintillation compound and may lose part of their energy to the  ${}^6\text{LiF}$  and binder before exciting the ZnS(Ag). Therefore, the number of photons produced per neutron interaction may vary depending on the scintillator mixture ratio and the grain size of the components. Furthermore, since ZnS(Ag) is not transparent to its own luminescence, adding too much of it will cause a major decrease in scintillator clarity leading to a very small light collection efficiency. The binder inside the scintillator is responsible mainly for holding all the components together, but the addition of more binder to the scintillator also increases the transparency of the scintillator. The WLS Fibers are responsible for light collection from the scintillator but adding too many fibers decreases the neutron capture efficiency and the scintillator light yield. To get the best detector performance for the desired detector dimensions and neutron energy, it is necessary to simultaneously optimize the composition and arrangement of the abovementioned components (Table 1). For the sake of further discussion, we will refer to the scintillator composition using a three-part ratio shorthand corresponding to the weight fraction of the principal components of  ${}^6\text{LiF}$  neutron converter, ZnS(Ag) phosphor, and the organic binder holding them together (e.g., LiF:ZnS(Ag):binder, 1:2:0.6).

To determine the optimal composition and configuration of the detector, we must establish a process for a guided exploration of these variables. A model of the system validated by empirical measurement then becomes a useful tool in evaluating many different detector configurations, leading to the production of the most promising prototype detectors.

GEANT4 (GEometry ANd Tracking) [14] is a platform for the simulation of the passage of particles through matter using Monte Carlo methods. The simulation was developed by CERN as an open source code toolkit. GEANT4 includes facilities for handling geometry, tracking, detector response, run management, visualization and user interface. It can realistically model the optics of scintillation including the light photon production and light transport considering its attenuation and reflection. The capability of GEANT4 to track both nuclear and optical processes was the reason for selecting this simulation platform for the optimization.

## 2. Optimization process

Our goal is to find a correlation between measurements of different detector configurations and their corresponding simulations. Upon finding this correlation, we can simulate many other detector configurations and estimate their total neutron detection efficiencies.

Simulating the entire detector requires that we estimate several important parameters. Some can be determined by conducting dedicated

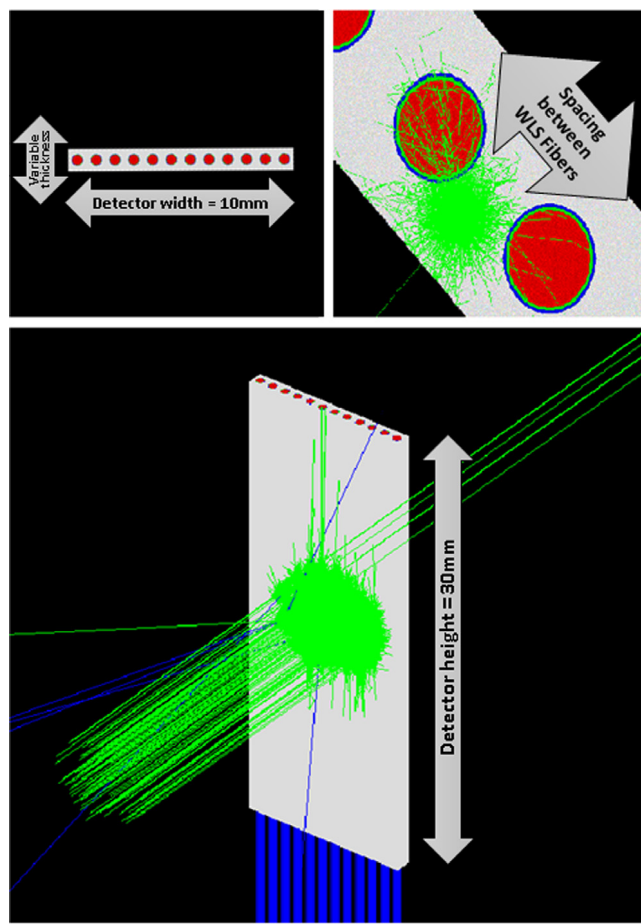


**Fig. 1.** The anatomy of the CANDOR neutron sensitive detector. The element consists of a slab of  ${}^6\text{LiF}:\text{ZnS}(\text{Ag})$  scintillator in which WLS fibers have been embedded. The WLS fibers serve to conduct scintillation light out of the plane of the detector to a photosensor. The height of the element is 30 mm and its width is 10 mm. The thickness is variable for the purposes of this discussion but is constrained near 1 mm.

simulations that provide us with information about the behavior and properties of the scintillator. Other parameters which could not be simulated were either measured empirically or approximated analytically. Parameters required for this simulation are the neutron capture efficiency, the light yield, and the optical transmission properties of the scintillator medium.

The steps we followed to optimize the scintillator is described graphically in Fig. 2 and in more detail in Sections 2.1 through 2.4 below.

- I. Neutron capture efficiency was measured and compared to simulations for numerous scintillators. We define this quantity as the number of neutrons passing through the detector which are absorbed by the medium. Discrepancies between measurement and simulation were determined (and confirmed by the manufacturer) to be caused by presence of air bubbles in the mixture formed during the manufacturing process. This affected both the neutron capture probability and light transport. By correcting for this, we could successfully produce simulation results that effectively matched measured results for the neutron capture efficiency for 1 mm thick scintillators containing WLS fibers.
- II. Optical properties were measured for different scintillator sheets using a LAMBDA 950 instrument allowing us to determine the optical absorption coefficients and Rayleigh scattering for each scintillator mixture for incorporation into the final simulation.

**Table 1**

There are four main components that determine the detector sensitivity. The portion of each component in the limited detector volume should be optimized based on its individual contribution to the neutron capture probability, the light yield, and light transport.

Component	Contribution to neutron capture	Contribution to light production	Contribution to light transport
<sup>6</sup> LiF	Increase	Decrease	Decrease
ZnS(Ag)	Decrease	Increase	Decrease
Binder	Decrease	Decrease	Increase
WLS fibers	Decrease	Decrease	Increase

- III. The light yield of each scintillator mixture was estimated through simulation, using ZnS(Ag) grains inside the scintillator according to their relative mass ratio and inspecting the amount of energy that was transferred to them [15]. Multiplying the literature value for ZnS(Ag) light yield of 100,000 Photons/MeV by the amount of energy transferred to the ZnS(Ag) in the scintillator provided the estimated light yield.
- IV. The minimum photon threshold for event discrimination was determined. A full simulation was conducted implementing all the measured parameters which allowed us to find the minimal photon threshold required for neutron signal detection. This photon threshold is similar to that found in the measurements conducted for all three detectors.
- V. The optimum spacing of wavelength shifting fibers in the scintillator was determined by finding correlations between simulations and measured results for three detector configurations. We simulated a configuration in which the WLS fibers were touching and which included reflectors on the outside surfaces of the scintillator slabs. Such an arrangement should simplify the manufacturing process. We predict the neutron sensitivity of this arrangement to be 88.6% for 4.75 Å neutrons using a 1:2:0.6 mixture ratio scintillator 1.05 mm thick with 20 WLS fibers and a Vikuiti reflector [16].
- VI. The optimal thickness of the detector was determined to meet the desired sensitivity.
- VII. The optimal size of LiF and ZnS grains was determined through simulation. Experimental observations followed by Scanning Electron Microscope imaging revealed that small grains can cluster to create grain sizes which are effectively larger than the nominal stock material.
- VIII. Once the correlation between simulation and experimental observation was established, other refinements to the design could be explored to enhance the overall neutron sensitivity.

### 2.1. Neutron capture efficiency

The scintillator is a multi-component mixture in which the active material for neutron capture is <sup>6</sup>Li. Because the design goal is to have an ultra-thin detector, the material must have a sufficient concentration of <sup>6</sup>Li to achieve the desired neutron capture efficiency. For this reason, we simulated the neutron capture probability for different scintillator mixtures and thicknesses. We simulated a scintillator block with 30 mm height, 10 mm width, and varying thicknesses in vacuum. A cold neutron beam with a cross sectional diameter of 6 mm was projected in to the detector. The absorption was estimated for each mixture and thickness using the mean neutron wavelength in the array (3.27 meV).

Two physics lists [17] were used for the simulation calculations and the results were compared. Both physics lists are dedicated to High Precision Neutrons:

**QGSP\_BERT\_HP**: Contains standard EM processes and uses **BERT**ini cascade for hadrons of energy below ~10 GeV; it is also used for neutrons below 20 MeV and is considered a **High Precision** neutron model.

**QGSP\_BIC\_HP**: Contains standard EM processes and uses **Binary** Cascade, pre-compound and various De-excitation models for hadrons; it is used for neutrons below 20 MeV and is considered a **High Precision** neutron model.

We have simulated several configurations with different widths and <sup>6</sup>LiF:ZnS(Ag):Binder weight fractions. It can be seen in [Table 2](#) that a thickness of 0.5 mm is sufficient for 90% neutron capture probability at the average neutron energy for all three mixtures. Since the overall detector thickness is about 1 mm and the WLS outer diameter is 0.5 mm, the minimal path for a cold neutron through the scintillator would be 0.5 mm granting us the required intrinsic neutron capture efficiency.

After validating that the desired scintillator thickness has sufficient neutron capture efficiency and therefore the feasibility for providing the required detection sensitivity, three frames of scintillator with different binder ratios were fabricated, each with a thickness of 1.0 mm and with 12 embedded WLS fibers. To measure their neutron capture efficiency, they were placed in front of a <sup>3</sup>He detector and were subjected to a direct neutron beam. By comparing the <sup>3</sup>He detector reading with and without the frames, the neutron absorption for each frame was calculated. A simulation calculating the neutron capture in the scintillators was conducted following the experiment described above.

A comparison between the simulation and the test results is shown in [Table 3](#). The table demonstrates that for both the simulation and the measurements, there is a decrease in the scintillator neutron capture efficiency as the proportion of binder concentration is increased.

We noticed that in the simulation, the neutron capture efficiency is higher than in the tests (e.g. 95% from simulation vs. 91% measured for a scintillator weight ratio of 1:2:0.6). We believe the cause for discrepancy is that when the scintillator is manufactured, air voids are created which lower the neutron capture efficiency. These assumptions were later confirmed by the scintillator manufacturer.

The correlation achieved between the simulation results and the measured data by adding air to the scintillator volume can be seen in [Table 4](#). We have calculated that an average of about 0.012% of air mass should be added to each of the scintillation mixture (21% air by volume).

### 2.2. Estimation of scintillation light yield

The final simulation requires an understanding of the light yield and its distribution for each scintillator mixture. We developed a simulation to obtain these two parameters.

Simulation of the maximum free path for alpha and triton particles in the scintillator and its compounds is necessary to determine the effect of the ZnS(Ag) grain size on light yield. For this simulation we modeled 10 cm × 10 cm × 10 cm blocks of ZnS(Ag), <sup>6</sup>LiF, binder and scintillator compound. A point source was placed in the center of each block which isotropically emits alpha and triton particles with their corresponding energies. All the events in which the particles passed their entire energy to the scintillator blocks were recorded and analyzed. The results were compared to SRIM [18] showing a good match.

From analyzing the path of alpha and triton particles in matter (see [Fig. 3](#)), it was observed that while triton particles can travel a substantial distance (~32 μm in ZnS(Ag) and <sup>6</sup>LiF and ~51 μm in the binder), the alpha particles only travel ~7 μm in ZnS(Ag) and <sup>6</sup>LiF and ~9 μm in the binder. From this we learned that increased proportions of binder in the mixture will result in less energy transferred to the ZnS(Ag) grains with a correspondingly lower light yield. Because the alpha particle only travels a relatively short distance, it is more important that the LiF and ZnS(Ag) grains be uniformly distributed. Clustering of either of these

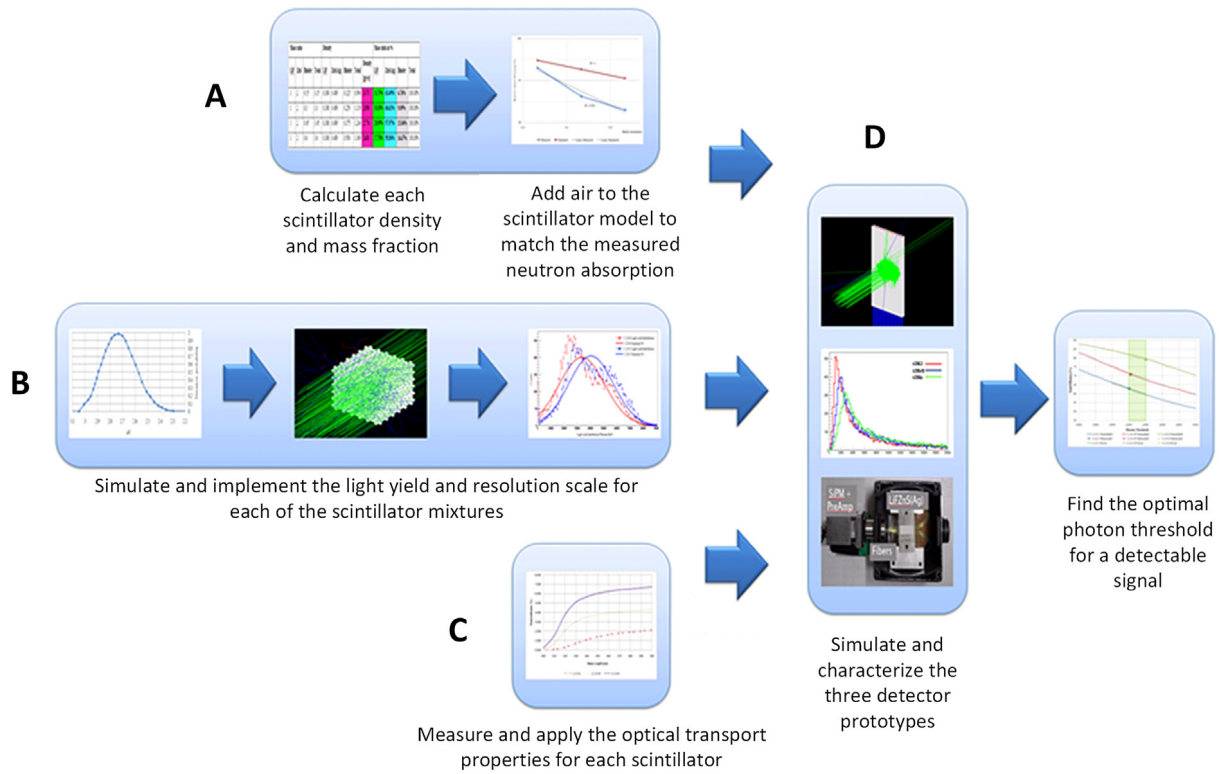


**Fig. 2.** A pictorial representation of the simulation process. We simulated (A) neutron capture in the scintillator, (B) light production as a result of neutron capture events, and (C) light transport in the scintillator to determine important parameters for a full scale simulation of the system (D).

**Table 2**  
Neutron capture efficiency (Percentage of neutrons interacting with the detector) using two different physics lists.

Mixture Thickness (mm)	Neutron capture efficiency using QGSP_BERT_HP [%]			Neutron capture efficiency using QGSP_BIC_HP [%]		
	1:2:0.3	1:2:0.45	1:2:0.6	1:2:0.3	1:2:0.45	1:2:0.6
0.25	76.7	72.8	69.7	76.3	72.8	69.7
0.50	<b>94.3</b>	<b>92.5</b>	<b>90.4</b>	<b>94.1</b>	<b>92.4</b>	<b>90.5</b>
0.75	98.3	97.5	96.6	98.3	97.6	96.6
1.00	99.3	99.0	98.6	99.3	99.0	98.5

**Table 3**  
Measured sensitivity vs. simulated efficiency for a threshold level of 2300 photons. The errors is 3% while the standard deviation of the threshold is 2% (Variations between actual measurement and simulation can occur by clustering between the grains of the compound).

Mixture ratio	Number of fibers	Scintillator thickness [mm]	Reflector type	Measured sensitivity [%]	Simulated sensitivity [%]
1:2:0.3	12	1.00	Air	62.8	60.9
1:2:0.45	12	1.00	Air	69.0	69.4
1:2:0.6	12	1.00	Air	79.6	80.6

**Table 4**  
Scintillator properties before and after adding air to the mixture.

Mixture ratio	Neutron capture efficiency [%]			Mass portion [%]		Air volume percentage [%]	Scintillator density [g/cm <sup>3</sup> ]	
	Measured	Simulated without air	Simulated with air	<sup>6</sup> LiF:ZnS(Ag)	Air		Without air	With air
1:2:0.3	96.5	97.4	96.0	99.99	0.010	19	2.95	2.40
1:2:0.45	93.1	96.3	93.3	99.98	0.013	22	2.77	2.16
1:2:0.6	91.5	95.3	91.7	99.98	0.014	22	2.63	2.04

species will impair either neutron capture or the effective absorption of the heavy ions (and therefore the light yield).

The amount of energy transferred from the alpha and triton particles to the ZnS(Ag) grains upon each neutron capture event should be calculated. By multiplying the amount of energy by the ZnS(Ag) light yield [19], we can estimate the light yield of each mixture.

To simulate the energy transferred from the alpha and triton particles to each of the scintillator compounds, a special simulation configuration

was required. Because in GEANT4, a composite material made from other materials is represented as a single material, GEANT4 cannot define how much energy was transferred to each of the material compounds. To overcome this obstacle, two of the compounds were mixed together in the desired ratio and the third compound, the one of interest (i.e. ZnS (Ag)), was placed inside them as spherical grains with varying mass ratios as can be seen in Fig. 4. Each unit cell was made from a total of four grains where one whole grain is placed in the

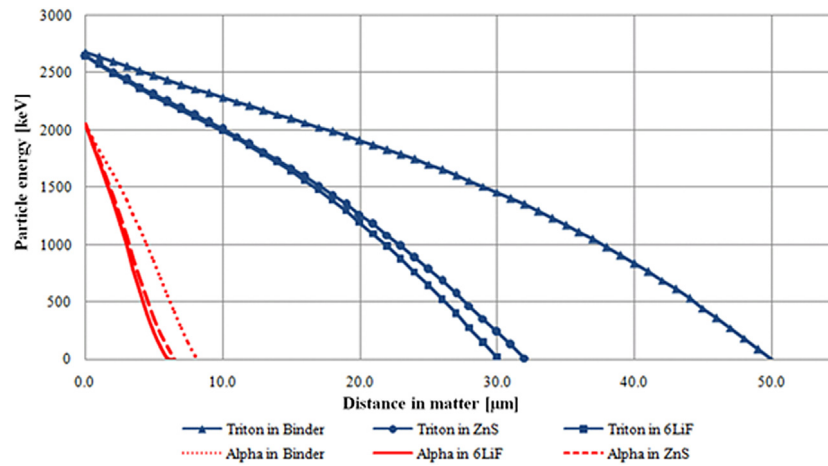


Fig. 3. Energy loss of an alpha and triton in matter; a triton has a long range in matter,  $\sim 30 \mu\text{m}$  to  $\sim 50 \mu\text{m}$ , while alpha particles have a very short range,  $\sim 6 \mu\text{m}$  to  $\sim 9 \mu\text{m}$ .

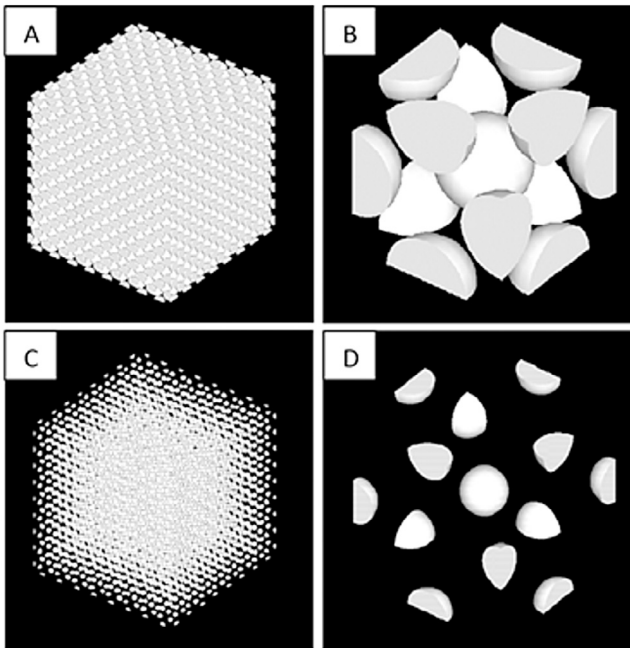


Fig. 4. (a) a matrix made of many unit cells containing high ZnS(Ag) mass ratio; (b) a single unit cell with high ZnS(Ag) mass ratio; (c) a matrix made of many unit cells containing low ZnS(Ag) mass ratio; (d) a single unit cell with low ZnS(Ag) mass ratio. Grain size is the same in all pictures. Cell size changed per mass ratio.

center and surrounded by twelve quarters. When placed in a 3D matrix, every quarter meets its neighbor from other unit cells to create a full grain.

Using the simulation, a volume containing vacuum was created and inside it was placed a  $1 \text{ mm} \times 1 \text{ mm} \times 1 \text{ mm}$  scintillator block made of many unit cells. Each unit cell is made of  ${}^6\text{LiF}$ , binder and air mixed together where ZnS(Ag) grains are embedded. A cold neutron beam with a  $0.3 \text{ mm}$  radius and a discrete energy of  $3.62 \text{ meV}$  ( $4.75 \text{ \AA}$  with fractional wavelength resolution  $\Delta\lambda/\lambda$  of 1%) was incident on the front of the scintillator block. To simulate an infinite scintillator, only events that transferred their entire energy to the scintillator were analyzed.

Alpha and triton energy deposition in each event were summed and stored for later analysis. By multiplying the deposited energy by the

ZnS(Ag) light yield and dividing it by the alpha and triton energy, we obtained the light yield distributions shown in Fig. 5.

A Gaussian fit was performed for each of the light distribution graphs giving us the mean values and standard deviation (sigma) for each of the scintillator mixtures. Using the standard deviation  $\sigma$ , and the mean scintillation value  $\mu_s$ , we calculated the resolution scale  $R_s$  for each of the scintillators per Eq. (1).

$$R_s = \frac{\sigma}{\sqrt{\mu_s}}. \quad (1)$$

The Resolution Scale parameter is the statistical fluctuation around the average yield. Values greater than 1 broaden the fluctuation and a value of zero produces no fluctuation.

After finding the resolution scale value, we simulated a simple scintillator with a given light yield and a calculated resolution scale value, and then plotted the emitted spectra to make sure our calculations are good.

We noticed (Fig. 6) that by adding more binder to the mixture, we linearly lower the scintillator light yield ( $\sim 10,000$  Photons/MeV decrease between 0.15 and 0.6 binder ratio) and increase the light yield resolution scale. From those two linear equations, we can calculate the light yield and resolution scale for any mixture of the type 1:2:binder where the binder ranges between 0.15 and 0.6.

We can see that in the 1:2:0.6 both light yield and resolution scale are worse than in the 1:2:0.15, but on the other hand, we must remember that by increasing the binder inside the scintillator, we dramatically improve optical transport.

### 2.3. Light transport in the scintillator

The optical properties of the material are defined by light absorption and the refractive indices. GEANT4 needs to know these parameters to fully simulate the scintillator. We obtained these numbers empirically.

The diffuse transmission of the scintillator plates was measured by placing a narrow light beam in front of the scintillator and counting the light reaching a very large sensor on the other side of the scintillator (covering its entire surface). These measurements were conducted at NIST using a LAMBDA 950 UV/Vis spectrophotometer [20]. Measurements were repeated for all the scintillator configurations using the relevant wavelengths (400 nm–500 nm) as can be seen in Fig. 7. The attenuation vector for each scintillator was calculated by isolating the attenuation coefficient  $\mu$  using Eq. (2) for each of the measured wavelengths.

$$I = I_0 e^{-\mu d}. \quad (2)$$

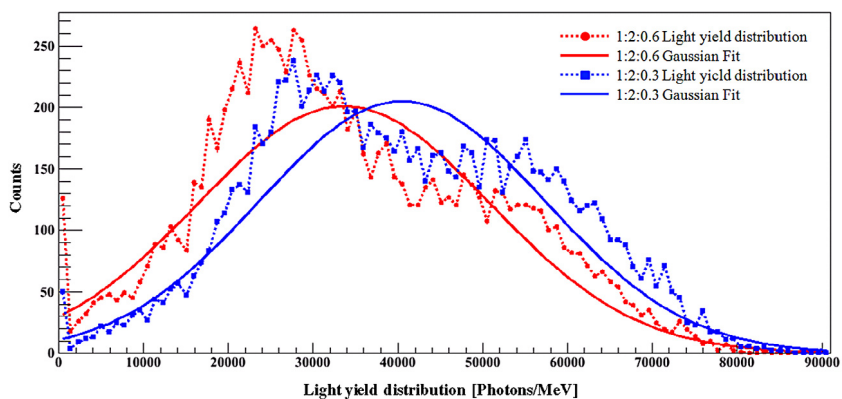


Fig. 5. Gaussian fitted light yield (photons/MeV) for two different scintillator weight ratios (<sup>6</sup>LiF:ZnS(Ag):Binder).

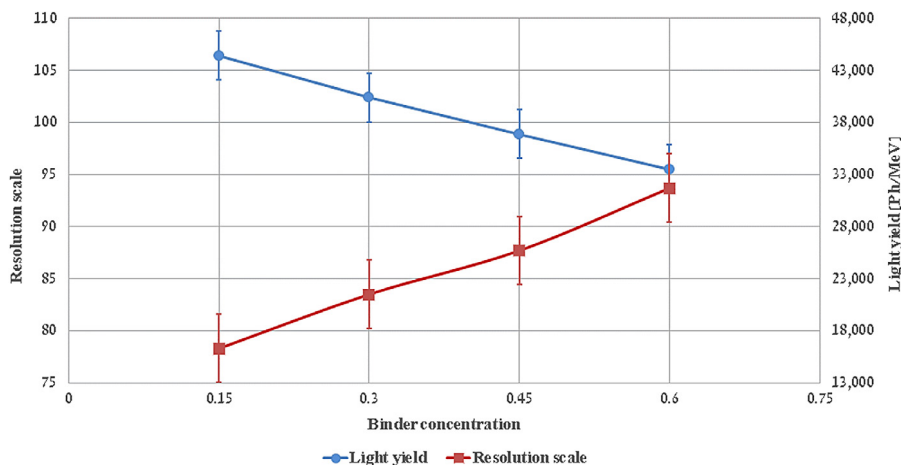


Fig. 6. Binder concentration dependent light yield and resolution scale.

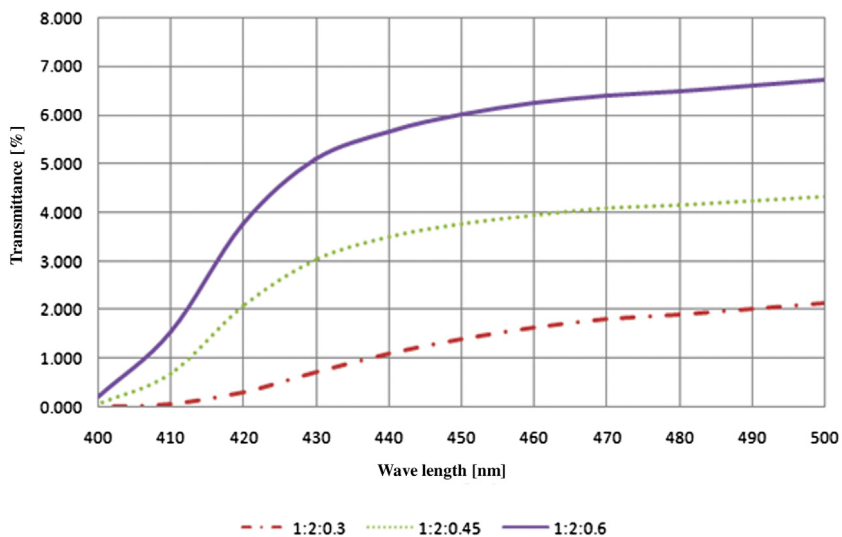


Fig. 7. Diffuse light transmittance through 0.43 mm thick scintillator slabs for three different scintillator stoichiometries.

The diffuse transmission measurements give us the number of photons that reached the other side of the scintillator, including photons that pass directly through, and photons that are Rayleigh scattered and still manage to reach the other side of the scintillator (traveling longer distances than the scintillator thickness). Therefore, these measurements give us a general but unique value which includes both the absorption

length and the Rayleigh scattering for each scintillator mixture. This calculated parameter was used in the simulation as the average distance traveled by a photon before being absorbed by the media.

Calculation of the scintillator refractive index was done according to the volume fraction of each of the mixtures multiplied by their refractive index (volume fraction mixing rule [21] for each of the

discrete wavelengths). Using Eq. (3) we calculated an approximate refractive index for each of the scintillator mixtures using the refractive indices of its four components multiplied by their volume fractions where “ $n$ ” is the refractive index of a material at a specific wave length and  $V$  is the volume percentage in the scintillator.

$$N = \frac{n_1 V_1 + n_2 V_2 + n_3 V_3 + n_4 V_4}{V_1 + V_2 + V_3 + V_4}. \quad (3)$$

When examining the calculated refractive index for a wavelength of 450 nm (the peak wavelength of the ZnS(Ag) luminescence) we noticed that there is no dramatic difference between mixtures. The values calculated for the mixtures are: 1:2:0.3 = 1.679; 1:2:0.45 = 1.623 and 1:2:0.6 = 1.597. Thus, the refractive index is not the dominant parameter responsible for differences in light attenuation between mixtures.

#### 2.4. Full scale simulation

In the final full simulation, we modeled a 10 mm × 30 mm × 1 mm scintillator detector containing WLS fibers and an “air” reflector. For each of the scintillator compounds, a block of the scintillation material with its relevant values such as density, light yield, optical absorption, Rayleigh scattering, refractive index and emission spectra are implemented. The detector was placed in front of a 0.6 mm diameter cold neutron beam with a discrete energy of 3.62 meV. For each neutron capture, we measured the total number of photons that entered the WLS fiber core. A spectrum of the collected photons was then tabulated. We also checked each spectrum for how many events there are for different photon threshold levels for comparison with real scintillator measurements. The empirical spectra scintillator mixtures of 1:2:0.3 and 1:2:0.45 containing twelve evenly distributed WLS fibers were compared with normalized simulated spectra under the same conditions.

Histograms of light yield are presented in Fig. 8 are for three different scintillator mixtures. The same number of neutrons was projected on each of the scintillators and the displayed spectrum is only for the neutrons that interacted with the scintillator. A photon threshold appropriate to the actual measured sensitivity for all three mixtures was then defined. Fig. 9 presents the detection efficiency versus the light photon threshold. When the threshold is set to zero, the 1:2:0.3 mixture has the highest efficiency because it has the highest neutron capture probability, but as the photon threshold increases the mixtures with better optical properties gain an advantage. Setting a photon threshold of 2300 photons provides good correspondence with the measured sensitivities for all three mixtures (Table 4) with error up to 3%, which is in range of two standard deviations for the light photons. This was then the value selected for the trigger. Put it context, the number of photons reaching the WLS fiber is reduced by 95% in transport to the SiPM for readout, and further reduced by the ≈25% quantum efficiency of the SiPM. This translates to a threshold at the photosensor of ≈25 photons, which is well above the dark noise of the SiPM.

We performed another study (Table 5) to find an overall thickness of the sensors that would yield the best light collection for the three mixtures. These configurations could become building blocks for multilayer detectors capable of detecting higher energy neutrons.

#### 2.5. Sensitivity improvements

Once we had established correlations between the simulations and experimental observations it was possible to explore additional refinements in the design to enhance neutron sensitivity.

The placement of the array of WLS fibers is also a tunable parameter. Fig. 10 shows a cross section of a portion of a detector. Each of the points represents a successfully processed neutron capture event (with a threshold of 100 photoelectrons). Most events (about 80%) are in the front half of the scintillator. This was true for all simulated mixtures. Because there is an asymmetry in distribution of neutron capture events

in the bulk of the scintillator, shifting the plane of fibers toward the front face of the detector can enhance the net neutron sensitivity of the device (Table 6).

Moreover, the closer an event is to the fiber the higher the amplitude of the light signal. For this reason, we believe that it is advantageous to position the plane of the fibers closer to the front face of the detector. Additionally, we recognize that no matter where a neutron capture event occurs, there should be a fiber in close enough proximity to capture the scintillation light.

We considered arrangements of WLS fibers in more than one plane within the scintillator. This project has focused on the use of a single layer of wavelength shifting fibers to keep the sensor as thin as possible. However, an alternative configuration with two layers of alternating fibers was demonstrated to yield higher neutron detection efficiencies.

Table 7 synthesizes a simulation whose goal was to determine the thinnest detector configuration with the highest neutron sensitivity. The alternating fiber configuration can deliver neutron sensitivities of about 95%.

In the simulations, we used an “air” reflector at the outside edge of the scintillator, where the boundary was defined as dielectric per the refractive indices of the scintillator and the air. Our study has shown the importance of improving the light collection from the interaction points that are located farther away from the WLS fiber. This can be achieved through the addition of reflector to direct scintillation light back into the medium. We used a dielectric–metal boundary where we set the reflectivity of the reflector according to the desired or the manufacturer’s specification. We have used three different values for the reflectivity: 0% to simulate absorption of the photons reaching the reflector; 98% to simulate the “Vikuiti” reflector; and 100% to simulate a perfect reflector.

By simulating a single WLS fiber coated with the scintillation material and clad with a reflector, we can determine the reflector contribution to light collection. We placed isotropic light sources at different distances from the fiber to calculate the amount of light reaching the fiber for reflectivities of 0%, 90%, and 100%. When the event is generated near the WLS fiber and far from the reflector, there is no contribution from the reflector, meaning that photons generated near the WLSF surface are either absorbed on the way back from the reflector or on their way to the reflector. For events occurring further away from the fiber, we can see that when a perfect reflector is used, the number of photons reaching the fiber from the detector edge is doubled compared to the case in which an absorber is used and is 43% higher than the case in which there is no reflector at all (the “air” reflector). Fig. 11 demonstrates that by adding a reflector, the number of light photons reaching the fiber increases for 60% of the neutron capture events in the scintillator.

### 3. Results

We investigated the ability to predict the sensitivity of new configurations based on simulations with selected parameters and using a photon threshold (entering the WLS fibers) of 2300 photons. We determined that a thicker detector containing about 50% more scintillator (1.35 mm) is required to ensure the robustness of our simulation. A high correlation is indicated by the 40.7% measured and the 40.6% simulated sensitivity for this configuration. Once we confirmed the reliability of the simulation for predicting neutron detection sensitivity, we started the process of optimizing the configuration of the detector using our results concerning the effect of external reflectors and fiber placement.

Simulation results for several different detector configurations are summarized in Table 8. Adding reflectors increases the predicted sensitivity from 79.6% to 85.1% and the measured sensitivity from 80.6% to 84.8%. Another configuration utilizing 20 fibers instead of 12 and a thickness of 1.22 mm instead of 1 mm (compensating for the added volume of the fibers) was simulated. The measured and simulated results for this configuration show a lower sensitivity (of about 78%). Therefore, the thickness was optimized (see Table 5) using simulation which shows a predicted sensitivity of 87.7% for a thickness of 1.1 mm without reflector and 89.5% with reflector.

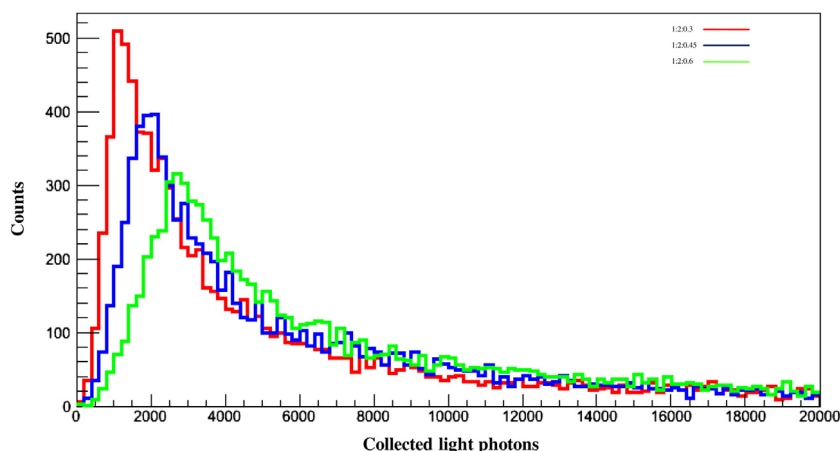


Fig. 8. Simulated spectra for three different scintillator mixtures: 1:2:0.3 (red), 1:2:0.45 (blue), and 1:2:0.6 (green). (For interpretation of the references to color in this figure legend, the reader is referred to the web version of this article.)

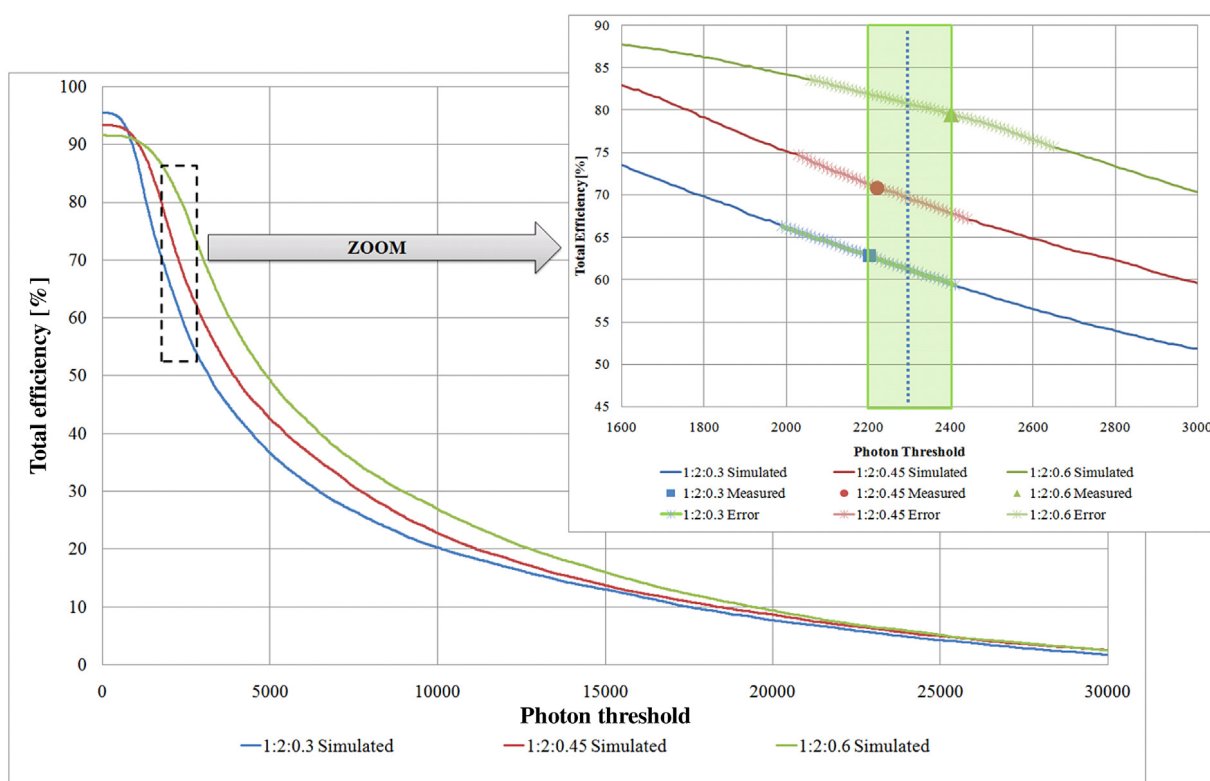


Fig. 9. Photon threshold graphs. As the photon threshold is increased the mixtures with better optical transmission permit better neutron discrimination. The photon threshold here was set to 2300 photons to match experimental observations.

Table 5

Suggested detector configurations with optimal light collection that can become a building block for a higher thermal energy detection configuration.

Mixture ratio	Number of fibers	Scintillator thickness [mm]	Neutron capture efficiency [%]	Light collection efficiency [%]	Total efficiency [%]
1:2:0.3	20	0.70	74.30	100	74.30
1:2:0.45	20	0.80	77.40	100	77.40
1:2:0.6	20	0.90	84.80	100	84.80

#### 4. Summary

This work presents a simulation developed with the intention of tuning the ratio of major components of a <sup>6</sup>LiF:ZnS(Ag) scintillator to achieve the best possible neutron detection efficiency with the thinnest detector. The net neutron detection efficiency is a function of the neutron capture efficiency determined by the <sup>6</sup>Li number density, the

light yield driven by the concentration of the ZnS(Ag) phosphor, the attenuation of the scintillation light within the medium tunable through the proportion of binder, and the efficiency of light collection which is enhanced by using external reflectors and the optimum arrangement of the WLS fibers. We relied on experimental measurements to determine values for several of the parameters required to simulate both the nuclear processes and the optical properties. After we selected an

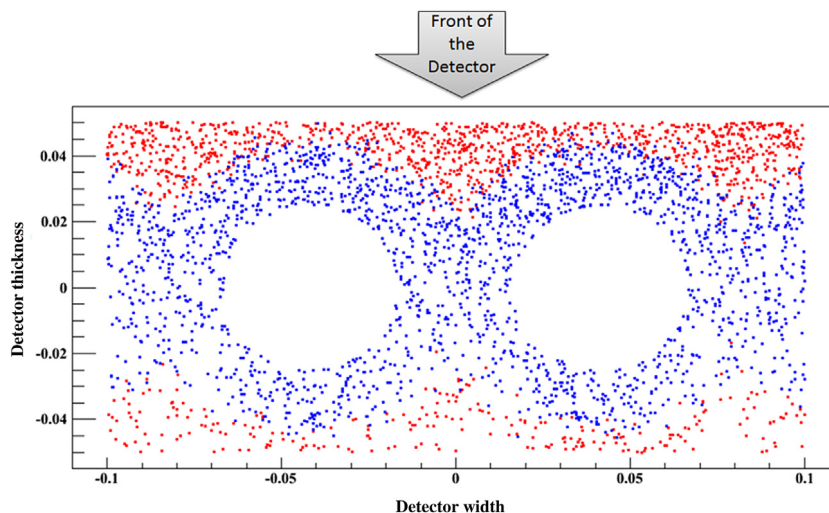


**Fig. 10.** Simulation of neutron capture in a cross section of a 1 mm thick detector with a 1:2:0.3 scintillator mixture. The red and blue dots represent neutron capture events which are successfully detected. The blue dots represent locations for which more than 3000 photons were collected inside the WLS fiber core. (For interpretation of the references to color in this figure legend, the reader is referred to the web version of this article.)

**Table 6**

Simulated efficiencies of a detector with a weight ratio mixture of 1:2:0.6, thickness 1.05 mm with Vikuiti reflector and 20 WLS fibers for an offset from scintillator center towards the front face of the detector.

WLS fibers offset [mm]	Neutron capture efficiency [%]	Light collection efficiency [%]	Total efficiency [%]
-0.20	90.2	45.0	40.6
-0.10	90.0	78.4	70.56
0.00	89.8	98.9	88.6
0.04	89.7	99.0	88.8
0.10	89.4	97.1	86.8
0.20	88.2	89.9	79.3

**Table 7**

Detector configuration with optimal sensitivity and thinnest dimensions without mechanical constraints such as spacing between the fibers and the number of fiber rows.

Scintillator mixture ratio	Number of fibers in a row (two rows)	Scintillator thickness [mm]	Neutron capture efficiency [%]	Light collection efficiency [%]	Total efficiency [%]
1:2:0.3	12	1.40	97.1	97.2	94.4
1:2:0.45	12	1.50	97.1	98.4	95.6
1:2:0.6	11	1.50	96.9	98.7	95.7

**Table 8**

A list of configurations tested for correlation between simulation and measured detector performance. The simulation optimized configuration had an 89.5% detection sensitivity with a 1.1 mm thickness, 20 fibers, external reflectors, and a 1:2:0.6 weight ratio.

Mixture ratio	Number of fibers	Scintillator thickness [mm]	Reflector type	Neutron capture efficiency [%]	Light collection efficiency [%]	Total simulated efficiency [%]	Measured efficiency [%]
1:2:0.6	12	1.00	Air	91.5	88.1	80.6	79.6
1:2:0.6	12	1.35	Air	97.2	41.8	40.6	40.7
1:2:0.6	12	1.00	Vikuiti	91.5	93.0	85.1	84.8
1:2:0.6	20	1.22	Vikuiti	93.2	85.1	79.3	77.7
1:2:0.6	20	1.10	Air	92.2	94.1	86.8	–
1:2:0.6	20	1.00	Vikuiti	87.6	97.8	85.7	–
1:2:0.6	20	1.05	Vikuiti	89.8	98.7	88.6	–
1:2:0.6	20	1.10	Vikuiti	92.1	96.0	88.4	–

appropriate photon number threshold we used the simulation to further refine the configuration of the detector.

The simulation provides insight on the key parameters which impact the performance of this new type of neutron proportional counter and which should be revisited as new configurations are evaluated. The stoichiometry of the scintillator should be reevaluated when either the desired detector thickness or the energy of neutron to be detected changes. Inclusion of an optical reflector on the outside surfaces can increase the proportion of photons emitted in the neutron capture

reaction which reach the wavelength shifting fiber and are ultimately detected by the photo sensor. Rearrangements of the WLS fiber used to collect the scintillation light can also increase the likelihood that neutron capture events with weak light amplitudes are successfully discriminated.

We have found several circumstances which can lead to discrepancies between the simulation and the experimental observations. Although in principle smaller grains of phosphor can improve the light yield, in practice these small grains can cluster to create a larger effective

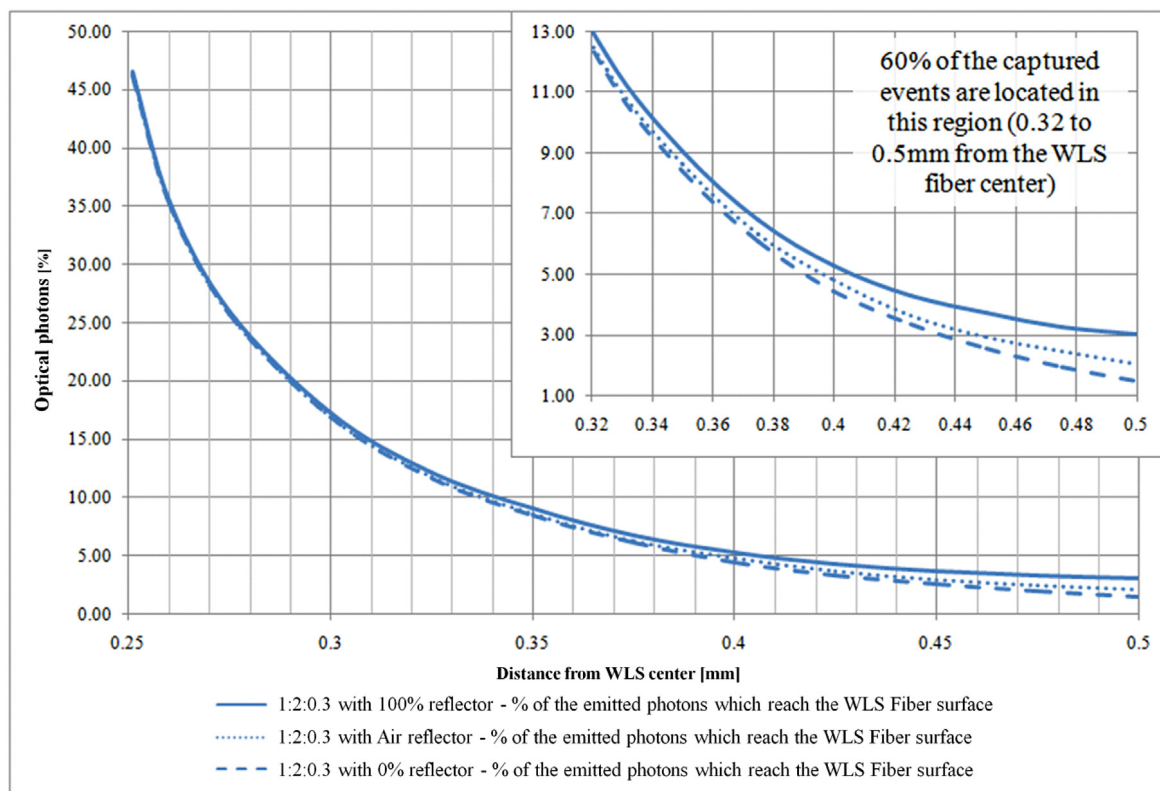


Fig. 11. Light collection efficiency vs. the distance from the neutron capture event. Adding reflectors to the outside face of the scintillator slab increases the number of photons which reach the WLS fiber.

grain size, resulting in less scintillation light. Displacing the plane of WLS fibers from the center of the detector toward the face can enhance light collection but can also result in more scattering from the hydrogen in the plastic, potentially leading to lower net sensitivity. Even varying the number of photons used as the trigger for discrimination can result in a change in detection sensitivity (two standard deviations for a threshold of 2300 photons can mean differences in efficiency of 2.8% for 1:2:0.3, 2.5% for 1:2:0.45 and 1.5% for 1:2:0.6). And finally, the photodetection efficiency of the photosensor itself, a function of working conditions such as the temperature and bias voltage, affect detection efficiency.

We predict that the high detection sensitivity achieved with the detector and the search for alternatives to  $^3\text{He}$  gas could lead to many more neutron detection applications based on the  $^6\text{LiF:ZnS(Ag)}$  scintillator. Although the applications will doubtless have requirements and constraints which differ from those for CANDOR, simulations such as those presented here can be a valuable tool for tuning the detector.

## 5. Disclaimer

Certain trade names and company products are identified to adequately specify the experimental procedure. In no case does such identification imply recommendation or endorsement by the National Institute of Standards and Technology, nor does it imply that the products are necessarily the best for the purpose.

## Acknowledgment

This work benefitted from the Center for Neutron Research at the National Institute of Standards and Technology; this facility is funded by the U.S. Department of Commerce.

## References

- [1] <http://www.ncnr.nist.gov/instruments/CANDOR>, [Online].
- [2] A. Stoykov, J.-B. Mosset, U. Greuter, M. Hildebrandt, A SiPM-based  $6\text{LiF:ZnS}$  scintillation neutron detector, *Nucl. Inst. Methods A* 787 (2015) 361–366.
- [3] A.C. Stephan, S. Dai, S.A. Wallace, Neutronics aspects of position sensitive neutron scintillator detectors using wavelength shifting readout fibers, *Appl. Radiat. Isot.* 61 (2004) 1375–1382.
- [4] A. Gorin, K. Kuroda, I. Manuilov, Development of a scintillation imaging device for cold neutrons, *Nucl. Inst. Methods A* 479 (2002) 456–460.
- [5] C.L. Melcher, Perspectives on the future development of new scintillators, *Nucl. Inst. Methods A* 537 (2005) 6–14.
- [6] A.N. Osovitzky, K.M. Pritchard, Y. Yehuda-Zada, J.B. Ziegler, E. Binkley, P. Tsai, A. Thompson, N. Hadad, M. Jackson, C. Hurlbut, G.M. Baltic, C.F. Majkrzak, N.C. Maliszewskij, Design of an ultrathin cold neutron detector, *Nucl. Inst. Methods A* (2018) Submitted for publication.
- [7] K.D. Ianakiev, M.T. Swinhoe, A. Favalli, K. Chung, D.W. MacArthur,  $6\text{Li}$  foil scintillation sandwich thermal neutron detector, *Nucl. Inst. Methods A* 652 (2011) 417–420.
- [8] W. Chong, B. Tang, Z. Sun, Q. Zhang, W. Luo, T. Wang, The Monte Carlo simulation on a scintillator neutron detector, *Sci. China Phys.* 56 (10) (2013) 1892–1896.
- [9] F. Pino, L. Stevanato, D. Cester, G. Nebbia, L. Sajo-Bohus, G. Viesti, Study of the thermal neutron detector  $\text{ZnS(Ag)/LiF}$  response using digital pulse processing, *J. Instrum.* 10 (2015) 8.
- [10] P. Dorenbos, “Scintillators for the detection of X-rays, Gamma Rays, and Thermal Neutrons,” 2010. [Online]. Available: <https://www.nikhef.nl/~d90/collegediktaat/scintillators.pdf>. [Accessed 2015].
- [11] H. Iwase, M. Katagiri, M. Shibayama, Optimization of the thickness of a  $\text{ZnS}/6\text{LiF}$  scintillator for a high resolution detector installed on a focusing small angle neutron scattering spectrometer, *Appl. Crystallogr.* 45 (2012) 507–512.
- [12] A.R. Spowart, Measurement of the gamma sensitivity of granular and glass neutron scintillators and films, *Nucl. Inst. Methods A* 135 (3) (1976) 441–453.
- [13] M. Katagiri, K. Sakasai, M. Masubayashi, Neutron/Gamma ray discrimination characteristics of novel neutron scintillators, *Nucl. Inst. Methods A* 529 (2004) 317–320.
- [14] S. Agostinelli, J. Allison, K. Amako, Geant4 - a simulation toolkit, *Nucl. Inst. Methods A* 506 (2003) 250–303.
- [15] A.N. Osovitzky, K.M. Pritchard, J.B. Ziegler, E. Binkley, Y. Yehuda-Zada, P. Tsai, A. Thompson, C. Cooksey, K. Siebein, N. Hadad, M. Jackson, C. Hurlbut, R.M. Ibberson, G.M. Baltic, C.F. Majkrzak, N.C. Maliszewskij,  $6\text{LiF:ZnS(Ag)}$  Mixture optimization

- for a highly efficient ultrathin cold neutron detector, *IEEE Trans. Nucl. Sci.* (2018) (in press).
- [16] (<http://multimedia.3m.com/mws/media/2857470/vikuiti-tm-ar-literature.pdf>).
- [17] D. Wright, “A Short Guide to Choosing a Physics List,” 2012. [Online]. Available: <http://geant4.slac.stanford.edu/MSFC2012/ChoosePhys.pdf>. [Accessed 2015].
- [18] J.F. Ziegler, M.D. Ziegler, J.P. Biersack, SRIM - The stopping and range of ions in matter, *Nucl. Inst. Methods B* 268 (2010) 1818–1823.
- [19] M.I. Arsaev, O.K. Bhelev, Energy dependence of the light yield of ZnS(Ag) luminophores (Phosphors), *Sov. At. Energy* 26 (1) (1969) 28–31.
- [20] Perkin Elmer, “Applications and Use of Integrating Spheres with the Lambda 650 and 850 UV/VIS and LAMBDA 950 UV/Vis/NIR Spectrophotometers,” 2015. [Online]. Available: [https://www.perkinelmer.com/CMSResources/Images/44-74191APP\\_LA MBDA650IntegratingSpheres.pdf](https://www.perkinelmer.com/CMSResources/Images/44-74191APP_LA MBDA650IntegratingSpheres.pdf). [Accessed 2015].
- [21] P. Chylek, V. Srivastava, R.G. Pinnick, R.T. Wang, Scattering of electromagnetic waves by composite spherical particles; experiment and effective medium approximations, *Appl. Opt.* 27 (1988) 2396–2404.